

Spin glass dynamics at the mesoscale

Samaresh Guchhait,^{1,*} Gregory G. Kenning,² Raymond L. Orbach,³ and Gilberto F. Rodriguez⁴

¹Microelectronics Research Center, The University of Texas at Austin, Austin, Texas 78758, USA

²Department of Physics, Indiana University of Pennsylvania, Indiana, Pennsylvania 15705, USA

³Texas Materials Institute, The University of Texas at Austin, Austin, Texas 78712, USA

⁴Department of Physics, University of California, Riverside, California 92521, USA

(Received 25 July 2014; revised manuscript received 9 December 2014; published 28 January 2015)

The mesoscale allows a new probe of spin glass dynamics. Because the spin glass lower critical dimension $d_l > 2$, the growth of the correlation length $\xi(t, T)$ can change the nature of the spin glass state at a crossover time t_{co} when $\xi(t_{co}, T) = \ell$, a minimum characteristic sample length (e.g., film thickness for thin films and crystallite size for bulk samples). For thin films, and times $t < t_{co}$ such that $\xi(t, T) < \ell$, conventional three-dimensional dynamics is observed. When $t > t_{co}$, a crossover to $d = 2$ behavior takes place. The parallel correlation length, associated with a $T_g = 0$ transition, increases in time from the saturated value of the perpendicular correlation length ℓ to an equilibrium value of the parallel correlation length proportional to $T^{-\nu}$. This results in a *pancakelike* correlated state, with a thickness ℓ and a temperature-dependent in-plane radius that increases with decreasing temperature. Activated dynamics is associated with these states. Measurements on Cu:Mn thin films are analyzed quantitatively within this framework. We extract a temperature-dependent activation energy from a fit to the frequency dependence of the dynamic susceptibility. The extrapolated temperature at which the activation energy would become large is close to the extrapolated glass transition temperature from ac susceptibility measurements. All known relevant experimental data are consistent with this approach. For polycrystalline materials, there is a distribution of length scales $\mathcal{P}(\ell)$. For sufficiently broad distributions, a logarithmic time dependence is derived for the time decay of the thermoremanent magnetization $M_{TRM}(t, T)$ using an approach originally derived by Ma. Properties dependent upon an effective waiting time t_w^{eff} are derived that are consistent with experiment, and further measurements are suggested.

DOI: [10.1103/PhysRevB.91.014434](https://doi.org/10.1103/PhysRevB.91.014434)

PACS number(s): 71.23.Cq, 75.10.Nr, 75.40.Gb, 75.50.Lk

I. INTRODUCTION

The time evolution of nonlinear dynamical systems depends strongly on initial conditions. For spin glasses, Zotev *et al.* [1] showed that the aging properties of a spin glass depend sensitively on the cooling protocol associated with arrival at the final measurement temperature. This behavior was explored at some length in the work of Rodriguez *et al.* [2]. They demonstrated the relationship between the cooling protocol and an effective waiting time t_w^{eff} .

Another initial condition to which attention has been drawn [3,4] is the relation of the magnitude of the spin glass correlation length $\xi(t, T)$ to a representative sample dimension ℓ . In a physical system prepared at times sufficiently short so that $\xi(t, T) < \ell$, the system behaves according to (spatial) dimension $d = 3$ dynamics. However, for preparation times greater than a crossover time t_{co} , defined through $\xi(t_{co}, T) = \ell$, the effective dimensionality is reduced. This reduction is of great significance for spin glasses in that the lower critical dimension $d_l > 2$ [5,6].

The advent of the *mesoscale* [7] allows these properties to be probed in real systems, allowing in principle the determination of the parallel (in-plane) correlation length exponent ν . This paper will be concerned with thin films, of the order of 20–30 Å thickness, and polycrystalline samples where the crystallite size is in the mesoscale range.

The experimental results for thin films form a remarkable series of papers, beginning with the Michigan State University

group [8,9] and culminating with their collaborators at Uppsala University [10,11]. Although these papers are now nearly 25 years old, they nevertheless hold promise for new studies that will further elucidate spin glass dynamics in reduced dimensionality. The results for polycrystalline materials are more recent, and illustrate the origin of the “end of aging” dynamically.

Our analysis is based on theoretical calculations [12–14] for the growth of the spin glass correlation length with time $\xi(t, T)$ and its experimental observation [15] for $d = 3$. In $d = 2$, the parallel spin glass correlation length grows rather slowly with time as calculated by Rieger *et al.* [16], then saturates at an equilibrium value proportional to $T^{-\nu}$ with the exponent $\nu = 3.6 \pm 0.02$ for Ising spin glasses [17], and $\nu = 0.9 \pm 0.2$ for Heisenberg spin glasses [18].

For short measurement times, the spin glass correlation length $\xi(t, T)$ is less than the film thickness, and the dynamics can be regarded as appropriate to $d = 3$. Under these conditions, it is found [12–14] that $\xi(t, T)$ grows as

$$\frac{\xi(t, T)}{a_0} = c_1 \left(\frac{t}{\tau_0} \right)^{c_2(T/T_g)}, \quad (1)$$

where a_0 is the average distance between magnetic spins, c_1 and c_2 are material-dependent constants, T_g is the spin glass transition temperature, and τ_0 is the average exchange time $\tau_0 \approx \hbar/(k_B T_g)$. The exponent c_2 is found to be very small, of the order of $0.12 < c_2 < 0.17$, depending upon the system [3]. As a consequence, $\xi(t, T)$ increases very slowly at long times, but it can reach thin film thicknesses within experimental time scales provided the temperature T is not too far below the

*samaresh@physics.utexas.edu

glass temperature T_g . Thus, as we shall show, the growth of $\xi(t, T)$ to a film thickness $\ell = 15.5$ nm (the length scale of Guchhait *et al.* [4]) for Cu:Mn (13.5 at.%) takes 5×10^5 s at $T = 0.83T_g$, and the age of the universe for $T = 0.5T_g$, while it takes only 5 ms for $\ell = 30$ Å (the length scale of Sandlund *et al.* [10]) at $T = 0.56T_g$.

At a given temperature, the $d = 3$ correlation length $\xi(t, T)$ grows to the film thickness ℓ at a time we designate as the crossover time t_{co} , changing the dimension from $d = 3$ to $d = 2$. At that point in time, the $d = 2$ parallel correlation length $\xi^{\parallel}(t_{co}, T)$ equals the perpendicular correlation length $\xi^{\perp}(t_{co}, T) = \ell$ [19]. If the temperature is subsequently lowered, $\xi^{\perp}(t, T)$ is fixed at ℓ while the parallel ($d = 2$) correlation length grows slowly [16] until it reaches its equilibrium value $\xi_{eq}^{\parallel}(T) \propto T^{-\nu}$.

The number of correlated spins encompassed by the perpendicular and parallel correlation lengths $\xi^{\perp}(t, T)$ and $\xi^{\parallel}(t, T)$, respectively, generates a distribution of free-energy barrier heights as a function of the Hamming distance between states, up to a maximum $\Delta_{max}(T)$ [3]. As shown in [20], the ultrametric relationship between states [21] separated by the barriers results in a temperature dependence for the barrier heights that causes a rapid growth (or diminution) as the temperature is lowered (or raised). Hence, in experiments where the temperature is changed during the experimental protocol, the initial temperature controls the subsequent dynamics. We term this initial temperature the “quench temperature” T_q .

Because the states are ultrametrically related, with state density increasing exponentially with increasing Hamming distance, the maximum barrier height reached after time t at temperature T , $\Delta_{max}(t, T)$, effectively controls the dynamics [4,20]. We relate $\Delta_{max}(T)$ to $\xi(T)$ in analogy to $d = 3$ [15] through

$$\frac{\Delta_{max}(T)}{k_B T_g} = \frac{1}{c_2} \left[\ln \left(\frac{\xi(t, T)}{a_0} \right) - \ln c_1 \right]. \quad (2)$$

In order to compare seamlessly with expressions appropriate to three dimensions, we define an effective correlation length $\xi^{eff}(t, T)$ for thin films by

$$\xi^{eff}(t, T) = \{\xi^{\perp}(t, T)[\xi^{\parallel}(t, T)]^2\}^{1/3}. \quad (3)$$

The $d = 2$ correlation length $\xi^{\parallel}(t, T)$ is presumed to grow on the time scale of experiment to its equilibrium value $\xi_{eq}^{\parallel}(T)$, so that for $t \geq t_{co}$, $\xi^{eff}(t \geq t_{co}, T) \equiv \xi^{eff}(T)$ is only a function of temperature T , remembering, of course, that $\xi_{eq}^{\parallel}(T)$ remains temperature dependent, proportional to $T^{-\nu}$.

Under controlled experimental conditions, the temperature is quenched to an initial value T_q . At that initial temperature, $\xi(t, T_q)$ grows with time until $t = t_{co}$ when $\xi(t_{co}, T_q) = \ell$, the sample thickness. After t_{co} , the system is *frozen* in a $d = 2$ state, with the largest barrier set entirely by the sample’s physical dimensions

$$\frac{\Delta_{max}(T = T_q)}{k_B T_g} = \frac{1}{c_2} \left[\ln \left(\frac{\ell}{a_0} \right) - \ln c_1 \right], \quad (4)$$

with both perpendicular and parallel correlation lengths $\xi^{\perp}(t \geq t_{co}, T_q) = \xi^{\parallel}(t \geq t_{co}, T_q) = \ell$. The only role of the quench temperature T_q is the rate at which $\xi(t, T_q)$ grows to ℓ from Eq. (1). The fact that Eq. (4) holds for different T_q arises

from the self-similarity of states at different temperatures, found experimentally over accessible temperature ranges in Refs. [4] and [20].

When the temperature is lowered from T_q , $\xi^{\parallel}(t, T)$ grows to $\xi_{eq}^{\parallel}(T)$, proportional to $T^{-\nu}$. This leads to

$$\xi^{eff}(t_{co}, T) = \{\ell[\xi_{eq}^{\parallel}(T)]^2\}^{1/3}, \quad (5)$$

and, concomitantly, through Eq. (2),

$$\frac{\Delta_{max}(T)}{k_B T_g} = \frac{1}{c_2} \left[\ln \left(\frac{\xi^{eff}(t_{co}, T)}{a_0} \right) - \ln c_1 \right]. \quad (6)$$

The combination of a maximum barrier height and exponential increase of the state occupancy with Hamming distance (and hence barrier height [22]) means that the dynamics after t_{co} will be Arrhenius type, with an exponent $\Delta_{max}(T)$ that is itself temperature dependent.

The temperature dependence of $\Delta_{max}(T)$ has a component in addition to the temperature dependence of ξ_{eq}^{\parallel} . This arises from the temperature dependence of the Hamming distance arising from the ultrametric tree for the free-energy states, associated with the temperature dependence of the Edward-Anderson overlap $q_{EA}(T)$ [15]. This has been measured explicitly through the temperature cycling experiments of Joh *et al.* [15]. In Sec. III of this paper, we shall assume that the increase in Hamming distance is associated with the correlation length $\xi^{eff}(t_{co}, T)$ through Eq. (5). An interpretation of the experiments of Kenning *et al.* [8,9] and Sandlund *et al.* [10] and Granberg *et al.* [11] on thin Cu:Mn films will be based on this analysis.

In the latter two papers, the dynamic susceptibility $\chi(\tau)$ was measured at different observations times τ ($\tau = 1/\omega$) for thin-film sandwiches of Cu:Mn 13.5 at.%, of thickness 30 and 20 Å, respectively, over a range of temperatures from the bulk value of the spin glass temperature T_g to low temperatures. The authors extrapolated the effective spin glass transition temperature $T_g^{eff} \rightarrow 0$ as the film thicknesses were reduced. What is different in our analysis is the interpretation that what was observed was the response of correlated spins within an effective volume $[\xi^{eff}(t_{co}, T)]^3$ through the arguments leading up to Eqs. (5) and (6).

This picture was invoked in a previous publication [4] to explain the time dependence of zero-field-cooled (ZFC) magnetization of (thicker) film of *a*-Ge:Mn [23], but at the quench temperature T_q . This paper extends their treatment to (thinner) films of Cu:Mn [8–11], and to temperatures below and above T_q .

For polycrystalline spin glasses with random crystallite length scales, we shall argue that the Ruderman-Kittel-Kasuya-Yoshida (RKKY) exchange coupling is cut off by finite crystallite length scales. This occurs even though the electrical conductivity generally is somewhat insensitive to polycrystallinity. The reason lies in the nature of the RKKY interaction itself. Its long-range and oscillatory nature is associated with the sharpness of the Fermi surface. However, as Kasuya calculates [24], electron scattering will change the long-range $\cos(2k_F r_{ij})/[k_F r_{ij}]^3$ dependence to $r_0/[(r_0^2 - r_{ij}^2)^2 + 4r_0^2 r_{ij}^2]$, where k_F is the Fermi wave vector, r_{ij} is the distance between spins i and j , and r_0 is a characteristic scattering length that we take to be of the order

of the crystallite size. The lack of an oscillatory character removes *frustration*, a requirement for spin glass behavior (in addition to randomness), and thus effectively decouples the individual spin glass grains.

In analogy with the previous discussion, this will limit the growth of $\xi(t, T)$ to a size characteristic of a particular spin glass crystallite. The distribution of crystallite sizes leads to a distribution of maximum barrier heights Δ_{\max} according to (4). The overall dynamics for a distribution of activation energies can be calculated using an expression originally introduced by Ma [25], and more generally by Amir *et al.* [26]. One finds a long-time logarithmic decay for the thermoremanent magnetization $M_{\text{TRM}}(t, T)$, first observed for spin glasses by Kenning *et al.* [27], but known for many other glassy systems (e.g. [28,29]). In addition, this model can be used to explain the very large times for overlap of the $M_{\text{TRM}}(t, T)$ decay curves at increasing effective waiting times t_w^{eff} , and the dependence of the crossover time t_{co} on t_w^{eff} , as observed in [27].

The next section will be a brief review of the dynamical spin glass properties to be explored in the paper in order to give the reader not familiar with spin glass notation sufficient background to access subsequent sections. Section III will treat the dynamics of uniform spin glass thin films, showing that the crossover to $d = 2$ behavior leads to activated dynamics with a temperature-dependent maximum barrier height as discussed above. Section IV addresses polycrystalline samples for random crystallite length scales, spanning a sufficiently broad range for the analysis of Ma [25] and Amir *et al.* [26] to be relevant. A logarithmic time decay for $M_{\text{TRM}}(t, T)$ is obtained, in agreement with the experiments of Ref. [27]. Section V analyzes the overlap of the very long-time behavior of $M_{\text{TRM}}(t, T)$ for different t_w^{eff} , and Sec. VI the dependence of t_{co} on t_w^{eff} . Section VII summarizes our results followed by our many acknowledgments.

II. BRIEF REVIEW OF DYNAMICAL SPIN GLASS PROPERTIES

The memory effect, typical of glasses in general, and of spin glasses in particular, arises from the cooling of the sample temperature from above the freezing temperature, referred to as the spin glass temperature T_g , to the measurement temperature T_q (which is here the same as the quench temperature defined before). It is assumed that the time to reach T_q is short (but see [2,30] for discussions of the effect of the cooling protocol). The time spent at T_q before the magnetic field H is changed is termed the waiting time t_w . The magnetic field change, either from $H = 0$ to the applied field H , leading to zero-field-cooled (ZFC) dynamics or from the applied field H to $H = 0$, leading to thermoremanent magnetization (TRM) dynamics, causes a change in the magnetic moment, the magnitude and time dependence of which depends upon t_w . The system exhibits, almost always, behavior characterized by an effective waiting time t_w^{eff} , larger than t_w , depending upon the cooling protocol [2,30]. The effective waiting time t_w^{eff} is typically extracted from the position of the peak in the relaxation function

$$S(t) = -\frac{1}{H} \frac{dM(t, T)}{d \ln t}, \quad (7)$$

where $M(t, T)$ is either the ZFC or TRM magnetization [31].

A physical interpretation of this phenomenon was introduced in Ref. [20] in terms of barrier hopping between degenerate free-energy phase-space states. The temperature dependence of a specific barrier was measured, and shown to increase rapidly as the temperature is lowered within a narrow temperature range of $\Delta T \approx 0.08$ K for Ag:Mn (2.6 at.%). For temperatures above T_q within this narrow temperature range $T_q + \Delta T > T > T_q$, small increases in temperature reduce barrier heights significantly, allowing diffusion to proceed more rapidly between states representative of those present at the measuring temperature T_q . Hence, this effective aging time t_w^{eff} , as derived from the peak position of $S(t)$, is larger than the actual waiting time t_w , the longer the cooling protocol finds itself within the narrow temperature range.

The works of Rodriguez *et al.* [2], and Parker *et al.* [30], examined the dependence of t_w^{eff} on the cooling path taken to reach T_q for Cu:Mn (6 at.%) (“Heisenberg type”); and CdCr_{1.7}In_{0.3}S₄, Au:Fe (8 at.%), and Fe_{0.5}Mn_{0.5}TiO₃ (all “Ising type”), respectively. While their interpretations are different, they provided clear evidence that the cooling path to reach T_q alters the magnitude of t_w^{eff} , even for $t_w = 0$. For this reason, the experiments of Kenning *et al.* [27] were conducted using the *fast cooling protocols* of Ref. [2], where the temperature after the quench is not allowed to rise above T_q . This keeps the occupied phase-space states within the same set of barriers appropriate to the effective aging time t_w^{eff} at T_q , or, equivalently, within the same spatial region spanned by $\xi(t_w^{\text{eff}}, T_q)$, minimizing t_w^{eff} for a given t_w . Using this protocol, one can safely work at longer times $t \gg t_w^{\text{eff}}$ to explore the consequences of $\xi(t, T_q)$ growing to sample dimensions. The end of aging is then associated with $\xi(t, T_q) \approx \ell$ at a fixed temperature T_q less than T_g at macroscopic length scales.

However, for mesoscopic length scales the form of Eq. (1) changes the growth dynamics. Thus, for $\ell \sim 30$ Å, as in the work of Sandlund *et al.* [10], $\xi(t, T_q) = \ell$ at 5 ms for $T_q = 37.5$ K ($T_g = 66.8$ K). This results in dynamics accessible within laboratory time scales, as will be discussed in the following section.

It is also important to understand the remarkable dependence of the growth rate of $\xi(t, T)$ on temperature from Eq. (1). Using the values for c_1 and c_2 from the literature [4,20], one finds that $\xi(t, T)$ grows very slowly for T significantly less than T_g , while for temperatures in the vicinity of T_g the growth is relatively rapid. Thus, as long as the temperature is significantly below T_g , $\xi(t, T)$ will never reach ℓ on laboratory time scales, and spin glass dynamics is appropriate to $d = 3$. However, in the vicinity of T_g , the reverse is true. For example, Ref. [4] finds $\xi(t, T) = \ell$ on laboratory time scales for 15.5 nm films of amorphous Ge:Mn in the narrow temperature range $0.83 < T/T_g < 0.92$ ($T_g = 24$ K). For $T < 20$ K ($T/T_g = 0.83$), the time required for $\xi(t, T) = \ell$ exceeds 4×10^5 s (reaching 3×10^6 s at 19 K, with $T/T_g = 0.79$), while for $T > 22$ K ($T/T_g = 0.92$), the time for $\xi(t, T)$ to reach ℓ is of the order of 10^4 s, a more accessible experimental time range. This limits dynamical measurement in practice to a rather narrow temperature range.

In summary, in order to prepare the spin glass sample for the purposes of extraction of dynamics in the time range where $\xi(t, T_q) \approx \ell$, it is necessary to work with as short a t_w^{eff} as possible, requiring a rapid cooling protocol wherein

the approach of temperature to the measuring temperature T_q never rises above T_q after quench, and either select a narrow temperature range below T_g for which $\xi(t, T_q)$ can approach ℓ for macroscopic samples, or work with materials of mesoscale dimensions for which $\xi(t, T_q)$ can approach ℓ over a wide temperature range.

III. SPIN GLASS DYNAMICS FOR UNIFORM THIN FILMS

As discussed in Ref. [4], when the spin glass correlation length $\xi(t, T)$ grows from nucleation at $t = 0$ to the thickness ℓ of a uniform thin film at $t = t_{co}$, the system crosses over from dimension $d = 3$ to $d = 2$ dynamical behavior. The latter is associated with a bulk $T_g = 0$ by virtue of the lower critical dimension for spin glasses $d_l > 2$ [5,6].

The earliest work on finite-size effects on the spin glass transition was performed on thin films of Cu:Mn (7 at.%) at a single effective time scale (inversely proportional to the temperature scan rate) in Refs. [8,9]. In that work, the spin glass thickness was changed in order to change the spatial dimension from $d = 3$ to $d = 2$ in order to probe the spin glass lower critical dimension d_l . The spin glass transition temperature T_g was measured over a range of thicknesses, ranging from 2 to 1000 nm. Extrapolations were introduced in order to demonstrate that $T_g \rightarrow 0$ as one approached $d = 2$. In subsequent work, a broad spectrum of observation times τ was extracted for 30 Å thin films of Cu:Mn (13.5 at.%) from the dynamic susceptibility $\chi(\tau)$ measured as a function of temperature at frequencies $\omega = 1/\tau$ for $10^{-5} < \tau < 10^4$ s in Ref. [10], while thin films of thickness 20 Å were probed over time scales of $10^{-4} < \tau < 10^3$ sec in Ref. [11] in a similar manner. A generalized Arrhenius law with a zero-temperature critical point was extracted for the very thin films. This was interpreted in terms of "... a crossover from three- to two-dimensional spin glass dynamics when one spatial dimension is gradually diminished to a finite size" [11].

However, as noted in Ref. [4], for times $t > t_{co}$ (when the transition from $d = 3$ to $d = 2$ dynamics has taken place) there will still remain correlated spins in the spin glass state, different from the interpretation of [8,9] and [10,11]. There will exist a maximum barrier height between metastable states for these states, the largest of which is given by Eq. (4) while at the quench temperature T_q . Because the degeneracy of the ultrametric space increases exponentially with Hamming distance, and because the barrier heights Δ are linearly proportional to the Hamming distance [22], dynamical properties will be determined through the largest barrier height Δ_{max} given by Eq. (4). This description remains until an external parameter is changed (e.g., temperature or magnetic field).

The data of Sandlund *et al.* [10] and Granberg *et al.* [11] for $\chi(\tau)$ versus temperature at different observation times τ allow a determination of the temperature dependence of $\Delta_{max}(T)$. In $d = 3$, the temperature dependence of a specific barrier can be determined [20], with $\Delta_{max}(T)$ increasing rapidly as the temperature is lowered from the quench temperature, as discussed in the Introduction. A fit to the measured data, when extrapolated to lower temperatures, produced very large values of $\Delta_{max}(T)$ that were well outside the experimentally accessible time window. This was speculated to lead to the

pure states of Parisi [32]. For $d = 2$, we shall show from the data of Ref. [10] that the correlated states also exhibit rapid barrier height growth as the temperature is lowered from the quench temperature T_q .

For temperatures accessed below the quench temperature, the increase of $\Delta_{max}(T)$ with decreasing temperature arises from two sources for thin films, as discussed in the Introduction. The first is associated with the growth of the Hamming distance as the temperature is lowered. The second is the growth in real space of the parallel correlation length $\xi^{\parallel}(t, T)$. This length grows slowly in time [16] from an initial value of $\xi_{eq}^{\parallel} = \ell$ at T_q , to an equilibrium value [19]

$$\xi_{eq}^{\parallel}(T) = \ell \left(\frac{T}{T_q} \right)^{-\nu} \quad (8)$$

for $T < T_q$. In the absence of explicit cooling times from Refs. [10,11], it is impossible to know if $\xi^{\parallel}(t, T)$ had reached its equilibrium value $\xi_{eq}^{\parallel}(T)$ within the time scale of the experiments. For purposes of analysis, we shall assume that sufficient time had elapsed in the experiments of Refs. [10,11] for $\xi^{\parallel}(t, T)$ to reach $\xi_{eq}^{\parallel}(T)$ as given by Eq. (8). Experiments sensitive to the growth of $\xi^{\parallel}(t, T)$ with time t is an area ripe for further investigation.

From the above arguments, we hypothesize that for decreases in temperature, the increase of $\Delta_{max}(T)$ arises from an increase in $\Delta_{max}(T)$ from Eqs. (5) and (6) plus an increase in the Hamming distance [20]. For increases in temperature, our hypothesis is different. The perpendicular correction length is pinned at the film thickness ℓ , effectively pinning the parallel correlation length also at ℓ [19]. The only change of $\Delta_{max}(T)$ with an increase in temperature is through the decrease in the Hamming distance, starting from the value $\Delta_{max}(T = T_q)$ from Eq. (4). In principle, the difference in the temperature dependencies of $\Delta_{max}(T)$ for temperatures below and above the quench temperature allows for the extraction of $\xi_{eq}^{\parallel}(T)$, and thus a direct measurement of the $d = 2$ critical exponent ν from Eq. (8).

We have employed the above analysis to extract $\Delta_{max}(T)$ from the experiments of Sandlund *et al.* [10] and Granberg *et al.* [11]. Their experiments measured the temperature dependence of the dynamic susceptibility $\chi(\tau)$ for different observation times τ for thin Cu:Mn (13.5 at.%) films of thicknesses 30 and 20 Å, respectively. The observation times $\tau(T)$ ranged over nine and seven orders of magnitude, respectively, in their respective Figs. 1(a). We extract $\Delta_{max}(T)$ from their measurements through the Arrhenius relation

$$\frac{1}{\tau(T)} = \frac{1}{\tau_0} \exp \left(- \frac{\Delta_{max}(T)}{k_B T} \right). \quad (9)$$

To extract parameters appropriate to their measurements, we use an average Mn spin separation appropriate to a concentration of 13.5 at.% of $a_0 = 4.45$ Å, and $T_g = 66.8$ K. We make use of the values for c_1 and c_2 for Cu:Mn (6 at.%) extracted by Joh *et al.* [15]: $c_1 = 0.653$ and $c_2 = 0.169$, on the assumption that these parameters are relatively insensitive to Mn concentration. Scaling $1/\tau_0$ from the 6 at.% Mn concentration of Joh *et al.* [15] to the 13.5 at.% Mn concentration of Sandlund *et al.* [10] and Granberg *et al.* [11] leads to $1/\tau_0 = 9.2 \times 10^{12} \text{ s}^{-1}$.

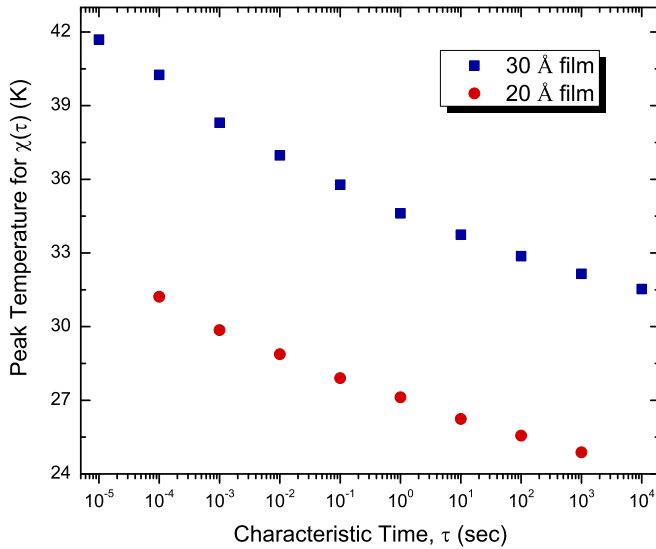


FIG. 1. (Color online) The temperatures for which $\chi(\tau)$ peaks are extracted from the plots of $\chi(\tau)$ versus temperature at different observation times τ , where $\tau = \omega^{-1}$, from Figs. 1(a) in Refs. [10,11], for Cu:Mn (13.5 at.%) films of 30 and 20 Å, respectively. The points at the higher peak temperatures (shorter τ) are less certain because of the broader experimental curves in this time regime.

The values for $\Delta_{\max}(T = T_q)$ from Eq. (4) can be extracted through a fit to the data of Refs. [10,11] for the two film thicknesses using the above parameters. We find $\Delta_{\max}(T = T_q) = 923$ K for $\ell = 30$ Å film, and $\Delta_{\max}(T = T_q) = 727$ K for $\ell = 20$ Å film. As stated above, these values are set by the film thickness, and are independent of temperature. The quench temperatures for these two films were not given in Refs. [10,11], so we extract them from a fit of Eq. (4) to the peak temperature of the dynamic susceptibility $\chi(\tau)$ for different observation times τ from the data exhibited in Figs. 1(a), respectively, of Refs. [10] and [11]. Figure 1 plots the temperatures of the peak of the measured $\chi(\tau)$ for each listed value of τ , as best we can extract them from the published figures. We find $T_q = 37.5$ K for the 30 Å film from the data of Ref. [10] and $T_q = 30$ K for the 20 Å film from Ref. [11].

The temperature-dependent $\Delta_{\max}(T)$ can be extracted by applying Eq. (9) to the temperature of the peak of $\chi(\tau)$ for each characteristic time τ , as exhibited in Fig. 1. We plot $\Delta_{\max}(T)$ in Fig. 2 for the 30 Å film, and in Fig. 3 for the 20 Å film. The difference of the dependence of $\Delta_{\max}(T)$ on temperature for the two films is striking. For the 30 Å film, $\Delta_{\max}(T)$ increases more rapidly than linearly with temperature as the temperature is lowered (exhibited by the departure from the “best fit to a linear relationship” line on Fig. 2). For the 20 Å film, the relationship of $\Delta_{\max}(T)$ to temperature is approximately linear (exhibited by the “best fit to a linear relationship” line on Fig. 3).

The data from which we have to work are rather sparse, but taking finite differences from Figs. 2 and 3, we plot the values for $\delta\Delta_{\max}(T)/\delta T$ against $\Delta_{\max}(T)$ for both film thicknesses in Fig. 4. The data for the 30 Å film in Fig. 4(a) are suggestive of a relationship similar to that found for bulk spin glasses [20] in that $-\delta\Delta_{\max}(T)/\delta T$ appears to rise rather

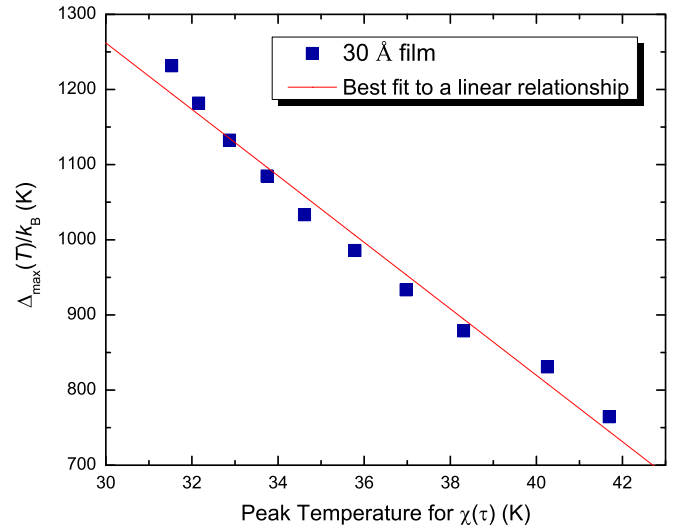


FIG. 2. (Color online) The temperature-dependent activation energy of the highest barrier $\Delta_{\max}(T)$ from Eq. (9) for the 30 Å Cu:Mn (13.5 at.%) film, plotted against the peak temperature for $\chi(\tau)$, using the data in Fig. 1. To guide the eye, a best fit to a linear dependence is plotted on the same graph. It is seen that there is a significant departure from a linear relationship between the values of $\Delta_{\max}(T)$ and the peak temperatures for $\chi(\tau)$ at the larger values of $\Delta_{\max}(T)$ (lower peak temperatures).

rapidly with increasing $\Delta_{\max}(T)$. The solid line is a fit to Eq. (10) below. The data for $\delta\Delta_{\max}(T)/\delta T$ for the 20 Å film in Fig. 4(b) are so scattered that it is difficult to draw any analytic conclusion except that $-\delta\Delta_{\max}(T)/\delta T$ does appear to increase with increasing $\Delta_{\max}(T)$.

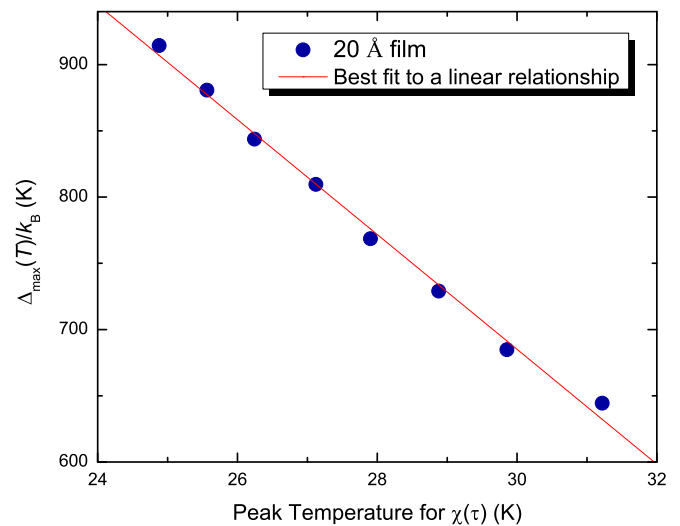


FIG. 3. (Color online) The temperature-dependent activation energy of the highest barrier $\Delta_{\max}(T)$ from Eq. (9) for the 20 Å Cu:Mn (13.5 at.%) film, plotted against the peak temperature for $\chi(\tau)$, using the data in Fig. 1. To guide the eye, a best fit to a linear dependence is plotted on the same graph. Some curvature could be imputed to the experimental points, but the data are too uncertain to claim anything else than a linear relationship between the values of $\Delta_{\max}(T)$ and the peak temperatures for $\chi(\tau)$.

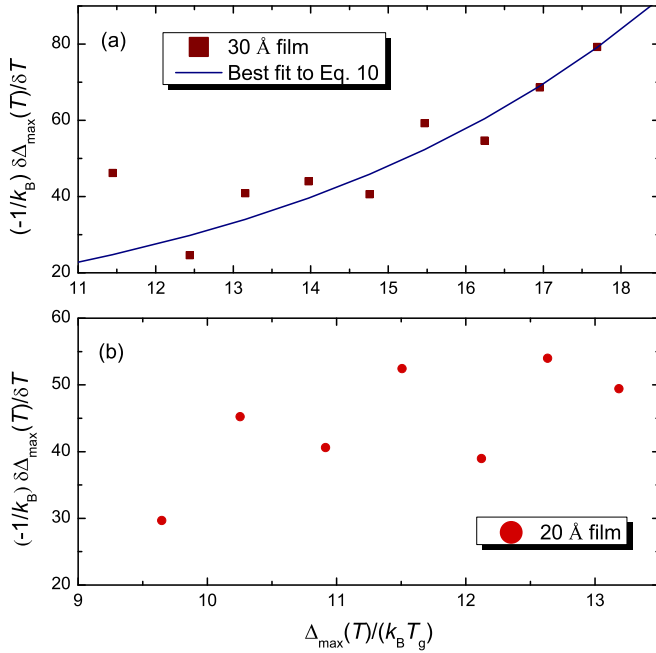


FIG. 4. (Color online) Plots of $\delta \Delta_{\max}(T)/\delta T$ against $\Delta_{\max}(T)$ extracted (a) from the data points for the 30 Å film from Fig. 2 and (b) from the data points for the 20 Å film from Fig. 3. The solid line for the 30 Å film in Fig. 4(a) is a fit of the 30 Å data to an exponential dependence of $\partial \Delta_{\max}(T)/\partial T$ on $\Delta_{\max}(T)$ [Eq. (10)] following the reasoning of Ref. [20]. The scatter for the 20 Å film in Fig. 4(b) obviates any fit.

Following the approach of Ref. [20], we fit the extracted data for $\partial \Delta_{\max}(T)/\partial T$ for the 30 Å film to an exponential form

$$-\frac{1}{k_B} \frac{\partial \Delta_{\max}(T)}{\partial T} = \alpha \exp \left[\frac{\beta \Delta_{\max}(T)}{k_B T_g} \right]. \quad (10)$$

In order to reduce the number of unknown constants, we make use of the value $\beta = 0.2$ from Ref. [20]. We find $\alpha = 2.18$ from a fit of Eq. (10) to the data in Fig. 4(a). The data exhibit some scatter around the fitted line, with the greatest scatter at the smaller values of $\Delta_{\max}(T)$ that occur at the higher temperatures. The experimental curves for the dynamic susceptibility $\chi(\tau)$ from Fig. 1(a) in [10] are broadest at the higher temperatures, so an accurate extraction of the temperature of the peak is more difficult in this region of temperature [and concomitantly for $\Delta_{\max}(T)$ at the smaller values]. The value of α (2.18) is approximately four times larger than the value of 0.5 from [20]. Noting that α in Eq. (10) is a scale factor representing the size of the barrier heights $\Delta(T)$, and that the Mn concentration to which we are fitting for Cu:Mn alloys is 13.5 at.% in Ref. [10], while the Mn concentration of Ref. [20] is 2.6 at.%, one would expect a ratio of approximately five from the concentration difference alone, as compared to four for the increase in α . The closeness of this scaling adds weight to our interpretation.

Integration of Eq. (10) leads to barrier heights increasing ever more rapidly as the temperature is lowered. The finite thickness of a thin film would mitigate against an infinite barrier height, but the fit in Fig. 4(a) to Eq. (10) certainly suggests much higher barriers for temperatures below those at

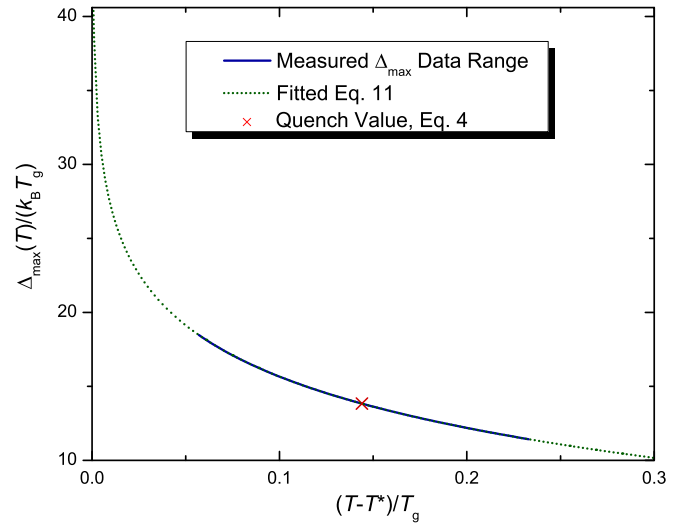


FIG. 5. (Color online) Integration of the exponential form for the dependence of $\partial \Delta_{\max}(T)/\partial T$ on $\Delta_{\max}(T)$ for 30 Å film, fitted to the experimental data (solid line portion), as a function of $(T - T^*)/T_g$, over the full range of $\Delta_{\max}(T)/(k_B T_g)$ and $(T - T^*)/T_g$ using Eq. (11). The \times denotes the value of Δ_{\max} at quench from Eq. (4).

the lowest experimentally accessible temperature. Integration of Eq. (10) leads to

$$\frac{\Delta_{\max}(T)}{k_B T_g} = -\frac{1}{\beta} \ln \left[\frac{\alpha \beta (T - T^*)}{T_g} \right] \text{ for } T > T^*, \quad (11)$$

where in principle $\Delta_{\max}(T)$ would diverge at $T = T^*$.

The fitted values $\alpha = 2.18$ and $\beta = 0.2$ for the 30 Å film are used to plot the magnitude of $\Delta_{\max}(T - T^*)$ versus the temperature difference $dT = T - T^*$ from Eq. (11) in Fig. 5. The dashed curve is Eq. (11), with the solid portion the extracted values of $\Delta_{\max}(T)$. The cross is at the position of the quench temperature T_q [equivalently, $\Delta_{\max}(T = T_q)$ from Eq. (4)]. The extrapolated divergence of $\Delta_{\max}(T)$ is predicted to take place at a $(T - T^*)/T_g \approx 0.06$ below the temperature of the lowest peak in [10], 31.5 K, leading to an extrapolated divergence of $\Delta_{\max}(T)$ at $T \approx 27.8$ K. The lowest experimental peak temperature is associated with $\tau = 10^4$ s. Going to any lower temperature, according to Eq. (11) plotted in Fig. 5, would lead to values of τ well beyond any experimental measurement range for $\chi(\tau)$.

As added evidence, Sandlund *et al.* [10] note that “there is a pronounced cooling rate dependence of the FC susceptibilities, with the knee shifting towards lower temperatures with decreasing cooling rate.” Associating the decrease in the cooling rate with an increase in τ is consistent with the growth of $\Delta_{\max}(T)$ as the temperature is lowered. The extrapolated value of $\Delta_{\max}(T)$ would represent an infinite time scale for τ , that would lead to a projected *knee* in the field-cooled (FC) magnetic susceptibility M_{FC}/H at $T = T^* \approx 27.8$ K.

The results for the 20 Å film are quite different. Figure 3, the plot of the $\Delta_{\max}(T)$ versus temperature, is approximately linear, displaying no noticeable increase beyond linear at the lower temperatures, and the scatter in Fig. 4(b) is so great that no analytic fit is possible. We suspect the difference of behavior from the 30 Å film is the relatively small number

of correlated spins even for times $t > t_{\text{co}}$ when $\xi(t_{\text{co}}, T_q) = \ell$. With the average distance between Mn spins equal to 4.45 Å, a spherical correlation volume with radius $\ell/2$ would contain only of the order of 50 spins in the 20 Å film, so that one might expect large spatial fluctuations for dynamical properties. This could be the origin of the scatter in Fig. 4(b). The 30 Å film contains of the order of 160 spins within a correlation volume at $t = t_{\text{co}}$ [$\xi(t = t_{\text{co}}, T_q) = \ell$] and can be thought of as a precursor to bulk. It would be of interest to probe the dynamical properties of films with thicknesses in the vicinity of 20 to 30 Å to probe the approach to bulk behavior as a function of the number of correlated spins.

It should be noted that the interpretations of Refs. [10,11] differ from our own, in that they associate their observed time scales with a generalized Arrhenius law using droplet scaling theory [33] for two-dimensional spin glass systems. Their analysis, on the assumption of a zero temperature transition [Eq. (3) of Ref. [10]] is based on

$$\ln(\tau/\tau_0) \propto T_f^{-(1+\psi\nu)}, \quad (12)$$

with T_f their “freezing temperature” associated with the maximum in the time-dependent susceptibility, and $\psi\nu = 1.6 \pm 0.2$. Our own analysis would yield a form more like that for critical dynamics [20]. Inserting (11) into (9), we find

$$\frac{\tau}{\tau_0} = \alpha\beta \left(\frac{T - T^*}{T_g} \right)^{-1/[\beta(T/T_g)]}. \quad (13)$$

This expression is of the usual critical exponent form [34], with $z\nu = 1/[\beta(T/T_g)]$. Using the value for $\beta = 0.20$, and taking T equal to the quench temperature 37.5 K, we find $z\nu \approx 9$. Further, from Fig. 5, we find a value for $T^* = 27.8$ K. The former is in rather remarkable agreement with experiments on three-dimensional spin glasses [35,36], and the latter with the value extracted using a critical slowing down analysis in [10] of $T_g = 26$ K.

Our analysis, based on spin glass correlations after $\xi(t, T)$ has reached the film thickness ℓ , appears consistent with all known relevant thin film and bulk experimental data.

IV. ORIGIN OF THE LOGARITHMIC TIME DEPENDENCE FOR TRM DECAY

In a polycrystalline sample, there is a distribution of crystallite sizes. As argued in the Introduction, this will introduce scattering into the integral responsible for the RKKY interaction, the oscillatory character of which is responsible for frustration that leads to spin glass behavior in dilute magnetic systems. The scatter changes the long-range oscillations to a uniform coupling falling off faster than the RKKY interaction [24]. This removes frustration and effectively decouples the spin glass states in the grains from one another, even though the electrical conductivity remains high.

The distribution of crystallite sizes, and hence of length scales ℓ , introduces dynamics that are more complex than for the uniform thin films treated in Sec. III. We denote the distribution of crystallite sizes through a probability distribution $\mathcal{P}(\ell)$, where ℓ is the length scale associated with a given crystallite. There exists, therefore, a maximum barrier height $\Delta_{\text{max}}(T = T_q)$ associated with each crystallite of length

scale ℓ from Eq. (4), that we designate as $\Delta_{\text{max}}(\ell)$. All of the experiments treated in this section will be at constant measuring temperature T_q , so that Eq. (4) uniquely determines $\Delta_{\text{max}}(\ell)$.

The distribution of length scales ℓ , governed by a probability density $\mathcal{P}(\ell)$, leads from (4) to a probability density for $\Delta_{\text{max}}(\ell)$ given by

$$\mathcal{P}(\Delta_{\text{max}}) = [\partial\Delta_{\text{max}}(\ell)/\partial\ell]^{-1} \mathcal{P}(\ell). \quad (14)$$

The purpose of this section is to derive the long-time dynamical properties for a polycrystalline spin glass. An example is the work of Kenning *et al.* [27] who displayed a logarithmic time dependence for the decay of the thermoremanent magnetization $M_{\text{TRM}}(t, T_q)$ at long decay times. We shall derive this property on the assumption that the measurement time scale is sufficiently long that each crystallite has crossed over into a low-dimensional state. That is, we assume that for each crystallite there is a crossover time t_{co}^ℓ , defined by $\xi(t_{\text{co}}^\ell, T_q) = \ell$, and that the measurement time $t > t_{\text{co}}^\ell$, for all ℓ .

The time development of $M_{\text{TRM}}(t, T)$ can then be deduced as follows. Upon removal of the magnetic field, all barriers are reduced in height by the change in Zeeman energy E_Z [37] (see the next section for more detail). The states occupied between barriers from $0 < \Delta < E_Z$ are instantaneously emptied into the lowest-energy Zeeman state (in our case, $M = 0$ for TRM decay). The remaining states then decay to the $M = 0$ state by transitions over the remaining barriers of height $0 < \Delta < \Delta_{\text{max}}(\ell) - E_Z$. For small changes in magnetic field, we can neglect E_Z with respect to $\Delta_{\text{max}}(\ell)$, so that the effective decay rate for a particle of size ℓ will be set by the largest barrier $\Delta_{\text{max}}(\ell)$. For waiting times short compared to the time for $\xi(t, T_q)$ to reach ℓ (we shall see that this condition is violated in some cases in Sec. VI), as the measurement time t increases, the TRM decay will cross over from conventional TRM decay to exponential for a given particle of length scale ℓ at measurement times $t > t_{\text{co}}^\ell$. We shall refer to the magnetization remaining at that time in the particle of length scale ℓ as $M_{\text{TRM}}^\ell(t > t_{\text{co}}^\ell, T_q)$. This leads to a size-dependent decay rate $1/\tau_\ell$ for $M_{\text{TRM}}^\ell(t > t_{\text{co}}^\ell, T_q)$ for a particular crystallite of length scale ℓ , where by generalizing Eq. (9)

$$\frac{1}{\tau_\ell} = \left(\frac{1}{\tau_0} \right) \exp \left[-\frac{\Delta_{\text{max}}(\ell)}{k_B T_q} \right]. \quad (15)$$

For a particle of length scale ℓ , $M_{\text{TRM}}^\ell(t > t_{\text{co}}^\ell, T_q)$ will then decay according to

$$M_{\text{TRM}}^\ell(t > t_{\text{co}}^\ell, T_q) = M_{\text{TRM}}^\ell(t_{\text{co}}^\ell, T_q) \exp(-t/\tau_\ell). \quad (16)$$

A polycrystalline sample consists of particles of length scale ℓ distributed through a probability density $\mathcal{P}(\ell)$. This requires that (16) with (15) be averaged over $\mathcal{P}(\ell)$. To make the average tractable, we shall replace $M_{\text{TRM}}^\ell(t_{\text{co}}^\ell, T_q)$ with an average $M_{\text{TRM}}(t_{\text{co}}, T_q)$ that will have to be extracted from experiment. We are then left with integrals of the sort

$$\int_0^\infty \exp(-t/\tau_\ell) \mathcal{P}(\ell) d\ell. \quad (17)$$

To make the evaluation more transparent, we use (14) with (15) to transform from $\mathcal{P}(\ell)$ to $\mathcal{P}(\Delta)$. The integrals are then of

the form, in an obvious notation,

$$\int_0^\infty \exp(-t/\tau_\Delta) \mathcal{P}(\Delta) d\Delta. \quad (18)$$

This class of integrals was first evaluated in this context by Ma [25]. For a flat distribution of barrier heights of width much greater than $k_B T_q$, (18) can be transformed to

$$\int_{k_B T_q \ln(t/\tau_0)}^\infty \mathcal{P}(\Delta) d\Delta. \quad (19)$$

We take $\mathcal{P}(\Delta)$ to be flat with width \mathcal{D} between $\Delta_0 - (\mathcal{D}/2)$ and $\Delta_0 + (\mathcal{D}/2)$, where Δ_0 is the mean value of Δ in $\mathcal{P}(\Delta)$, and we assume $\mathcal{D} \gg k_B T_q$, so that $\mathcal{P}(\Delta) = 1/\mathcal{D}$. Ma [25] evaluates this integral by noting that it is the area under $\mathcal{P}(\Delta)$ to the right of $(T_q/T_g) \ln(t/\tau_0)$. The part to the left of $(T_q/T_g) \ln(t/\tau_0)$ has already decayed. Then, the integral (19) is equal to

$$\frac{1}{\mathcal{D}} \left[\Delta_0 + \frac{\mathcal{D}}{2} - k_B T_q \ln\left(\frac{t}{\tau_0}\right) \right]. \quad (20)$$

Using (16) and (20), we now have

$$M_{\text{TRM}}(t, T_q) = \frac{M_{\text{TRM}}(t_{\text{co}}, T_q)}{\mathcal{D}} \left[\Delta_0 + \frac{\mathcal{D}}{2} - k_B T_q \ln\left(\frac{t}{\tau_0}\right) \right], \quad (21)$$

where $t > t_{\text{co}}^\ell$ for all ℓ . Taking the derivative with respect to $\ln t$ generates

$$\frac{\partial M_{\text{TRM}}(t, T_q)}{\partial \ln t} = -\mathcal{B} T_q^{(r)} M_{\text{TRM}}(t_{\text{co}}, T_q), \quad (22)$$

where \mathcal{B} is a constant containing the many factors associated with (22), $T_q^{(r)} = T_q/T_g$, and $M_{\text{TRM}}(t_{\text{co}}, T_q)$ is an average value of $M_{\text{TRM}}(t, T_q)$ over the various times t_{co}^ℓ [equivalently, an average of $M_{\text{TRM}}^\ell(t_{\text{co}}^\ell, T_q)$ over particle dimensions ℓ]. Experimentally, $M_{\text{TRM}}(t_{\text{co}}, T_q)$ will be taken to be the value of the TRM when the decay crosses over to $\ln t$ behavior.

The experimental data for $S(t)$ for Cu:Mn (6 at.%), at $T_q = 26$ K [$T_q^{(r)} = 0.83$], were reported in Ref. [27] and their Fig. 1 is reproduced here as our Fig. 6. The inset in Fig. 6(b) for the shortest effective waiting time (7 s) clearly displays a crossover to logarithmic behavior at approximately 1000 s, and continues for at least two orders of magnitude in time. Using the parameters from Joh *et al.* [3], one can calculate the value of the correlation length $\xi(t, T_q)$ to test the assumptions leading to Eq. (15). At $t = 10^3$ s, $\xi(10^3, 26 \text{ K}) \approx 60$ nm. At $t = 10^5$ s, $\xi(10^5, 26 \text{ K}) \approx 130$ nm. Rodriguez [2] estimated crystallite sizes ranging from 80 to 300 nm, with an average size of approximately 100 nm. Thus, in the time regime contained in the inset of Fig. 6(b), where logarithmic time behavior is exhibited, the correlation length is comparable to the length scale of the Cu:Mn crystallites, a condition required for the use of Eq. (15) for $1/\tau_\ell$. The broad range of crystallite length scales probed by $\xi(t, T_q)$ over this time scale is consistent with the approximations contained in the evaluation of Eq. (19).

It should be noted that logarithmic behavior at long times is not limited to spin glasses. For example, Amir *et al.* [26] find a rather ‘‘general mechanism for slow relaxations and aging, which predicts logarithmic relaxations...’’ and, in an extensive analysis of electron glass dynamics, find many examples of $\ln t$ behavior. In that sense, Eq. (22) may be a

specific manifestation of a more general relationship for glassy systems.

V. VERY-LONG-TIME BEHAVIOR OF $M_{\text{TRM}}(t, T)$

The previous section discussed the long-time behavior for polycrystalline spin glasses after crossover to $d < 3$, i.e., when the correlation length has reached the length scale of the crystallites. Figure 6(b) [reproduced from Fig. 1(b) of [27]] exhibits the subtraction of the $t_w^{\text{eff}} = 7$ s TRM decay curve for the fast cooling protocol from those at longer effective waiting times $17.5 \leq t_w^{\text{eff}} \leq 44$ s, all utilizing the fast cooling protocol, for polycrystalline Cu:Mn (6 at.%). The striking feature of these differences is the very long time for the various curves to cross over to the $t_w^{\text{eff}} = 7$ s value. For example, the long-time portion of the $t_w^{\text{eff}} = 17.5$ s decay curve overlaps the long-time portion of the $t_w^{\text{eff}} = 7$ s decay curve at an overlap time $t_{\text{ov}} \approx 6,000$ s, whereas the $t_w^{\text{eff}} = 44$ s and the $t_w^{\text{eff}} = 110$ s curves

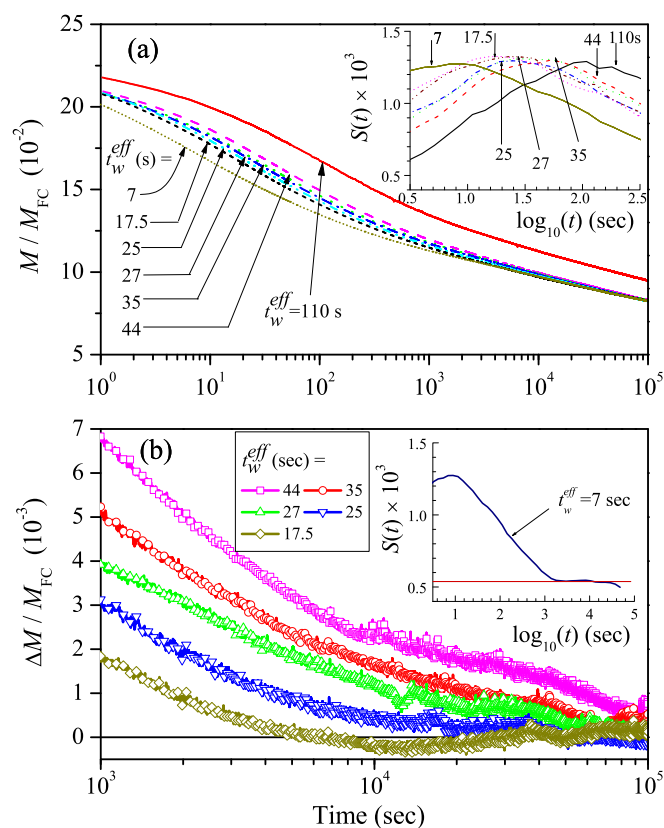


FIG. 6. (Color online) Reproduction of Fig. 1 from Ref. [27]. Figure 6(a) shows the decay curves for t_w^{eff} equal to 7, 17.5, 25, 27, 35, 44, and 110 s. In the inset, the relaxation curves $S(t)$ for each curve are used to determine t_w^{eff} . Figure 6(b) displays the subtraction of the $t_w^{\text{eff}} = 7$ s TRM decay curve from the other TRM curves. The $M_{\text{TRM}}(t)$ curve for $t_w^{\text{eff}} = 17.5$ s begins to overlap the $M_{\text{TRM}}(t)$ curve for $t_w^{\text{eff}} = 7$ s at a time $t_{\text{ov}} \approx 6000$ s, while the curve for $t_w^{\text{eff}} = 44$ s overlaps at a $t_{\text{ov}} \sim 10^5$ s, and by extrapolation the curve for $t_w^{\text{eff}} = 110$ s overlaps at a time $t_{\text{ov}} \sim 10^9$ s. The inset displays the relaxation curve $S(t)$ for the $t_w^{\text{eff}} = 7$ s curve. The curve becomes horizontal at $t \sim 10^3$ s, remaining flat over two orders of magnitude in time, indicating a crossover to a logarithmic time dependence for the decay of $M_{\text{TRM}}(t)$.

do not overlap at long times with the $t_w^{\text{eff}} = 7$ s decay curve until $t_{\text{ov}} \sim 10^5$ s and, by inference, 10^9 s, respectively.

We suggest that this striking dependence of the long-time behavior of the TRM decay upon t_w^{eff} is the result of the dependence of the initial magnitude of $M_{\text{TRM}}(t_{\text{ov}}, T_q = 0.83 T_g)$ on the effective waiting time t_w^{eff} . The highest barrier surmounted during a waiting time t_w^{eff} is given by Eq. (9) that we rewrite as

$$\Delta(t_w^{\text{eff}}, T_q) = k_B T_q (\ln t_w^{\text{eff}} - \ln \tau_0). \quad (23)$$

When the magnetic field is removed, measurements by Chu *et al.* [36], along with other observations of a similar nature by Vincent *et al.* [37], suggest that a change in magnetic field *reduces* the barriers in the initially occupied field-cooled magnetization manifold M_{FC} by the change in Zeeman energy E_Z . This reduction can be thought of conceptually as diffusion between states of constant M_{FC} through intermediate states of lower Zeeman energy [38]. States within the M_{FC} manifold with barriers less than the Zeeman energy change are emptied instantaneously into the $M = 0$ manifold [35,36]. The Zeeman energy change is given by

$$E_Z = N_s \chi_{\text{FC}} H^2, \quad (24)$$

where N_s is the number of spins within a correlation length that participate in barrier hopping {we shall set $N_s = [\xi(t_w^{\text{eff}}, T_q)/a_0]^3$ }, and χ_{FC} is the magnetic susceptibility *per spin* obtained from the total value of the field-cooled magnetic susceptibility M_{FC}/H divided by the total number of spins N .

From Eqs. (23) and (24), the larger t_w^{eff} , the larger the thermoremanent magnetization $M_{\text{TRM}}(t=0, T_q)$ remaining when the magnetic field is removed. That is, the fractional change $E_Z/\Delta(t_w^{\text{eff}}, T_q)$ diminishes as t_w^{eff} increases. This is seen explicitly in Fig. 6 where the initial value of $M_{\text{TRM}}(t=0, T_q = 0.83 T_g)$ increases as t_w^{eff} increases. Hence, in order for the long-time decay portions of $M_{\text{TRM}}(t, T_q)$ to become comparable in magnitude for differing values of t_w^{eff} , the offset

in the initial values of $M_{\text{TRM}}(t=0, T_q)$ must be overcome through the time decay of $M_{\text{TRM}}(t, T_q)$. But, the very slow decay of $M_{\text{TRM}}(t, T_q)$ for $t > t_{\text{co}}$, proportional to $\ln(t/\tau_0)$ from (21), means that this difference will take very long times, exponentially increasing with increasing t_w^{eff} . This dependence is exhibited in Fig. 7 where t_{ov} is plotted against t_w^{eff} .

VI. EFFECTIVE WAITING TIME DEPENDENCE OF t_{co}

It was pointed out in the Introduction that the crossover time to logarithmic time decay for $M_{\text{TRM}}(t, T_q)$ depends on the effective waiting time t_w^{eff} . This is caused by the growth of $\xi(t, T)$ during the waiting time. If, for example, $\xi(t, T)$ were to grow during t_w^{eff} to overlap some of the smaller crystallites, then when the magnetic field is removed, the smaller crystallites portion of $\mathcal{P}(\ell)$ (i.e., those with the smallest length scale ℓ) would have already have transitioned to $d < 3$. Then, as time progresses after removal of the magnetic field, it would appear that the mean of $\mathcal{P}(\ell)$ for which aging continues (i.e., for $d = 3$ dynamics) is shifted to larger ℓ . This would show up as an increase of t_{co} with increasing t_w^{eff} . It would be interesting to test this dependence experimentally. For example, in the Cu:Mn 6% sample used in the experiments of Rodriguez *et al.* [2], at $T_q/T_g = 0.95$, a waiting time of $t_w = 110$ s would yield $\xi(t_w = 110 \text{ s}, T_q = 0.95 T_g) = 86$ nm, just overlapping the smallest of the crystallites in his sample. For $t_w = 406$ s, $\xi(t_w = 406 \text{ s}, T_q = 0.95 T_g) = 106$ nm, already larger than the mean crystallite size of his sample. Thus, the system would contain effectively larger crystallites for crossover to logarithmic decay with increasing t_w^{eff} , hence a larger t_{co} for larger t_w^{eff} . Experiments remain to be performed over accessible time scales to check this prediction.

VII. SUMMARY

We have explored the dynamics for spin glasses at the mesoscale. For uniform thin films, we have exhibited how the crossover from $d = 3$ to $d = 2$ results in spin glass correlations with the perpendicular correlation length equaling the film thickness, while the parallel correlation length grows as the temperature is lowered. The ultrametric nature of these states generates a temperature dependence of the dynamics, consistent with the observed temperature dependence of the dynamic susceptibility $\chi(\tau)$ for a thin film of Cu:Mn (13.5 at.%) of thickness 30 Å [10]. We were unable to analyze the dynamics of the thinner film of thickness 20 Å [11] because of what we believe to be large spatial fluctuations associated with the relatively small number of spins within a correlated volume. For polycrystalline samples, we have derived an expression for the logarithmic decay of the TRM after the correlation length has become comparable to crystallite sizes. This behavior is nearly universal for glassy systems [28,29], and in this sense, spin glasses follow suit. The time for $\xi(t, T)$ to become comparable to crystallite dimensions falls within the experimentally accessible range for temperatures in the vicinity of T_g , but increases precipitously at lower temperatures. Finally, predictions are made with respect to the onset of the logarithmic decay of the thermoremanent magnetization (TRM) that should be explored.

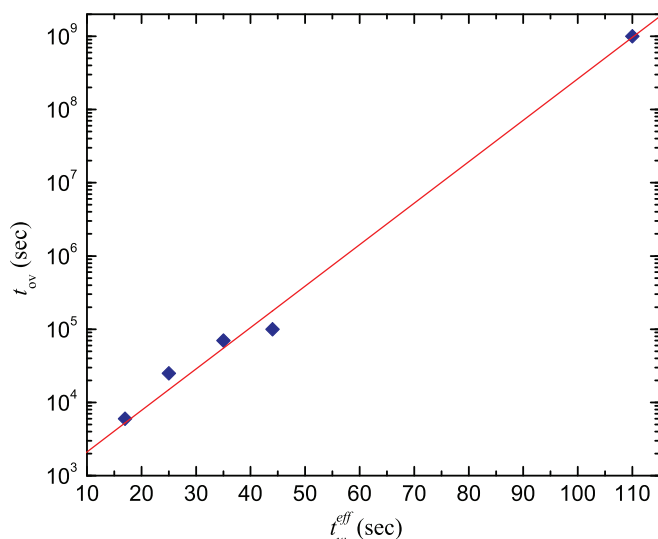


FIG. 7. (Color online) A logarithmic plot of the time for the $M_{\text{TRM}}(t)$ curves to overlap the $M_{\text{TRM}}(t)$ curve for $t_w^{\text{eff}} = 7$ s, as a function of their respective t_w^{eff} .

ACKNOWLEDGMENTS

The authors wish to acknowledge conversations with Dr. G. A. Henkelman, Dr. D. E. Makarov, and Dr. P. J. Rossky, an extensive discussion with Dr. D. R. Reichman, and detailed correspondence with Dr. F. Ritort. The authors are also indebted to Dr. M. A. Moore who first pointed out the importance of the growth of the parallel correlation length,

and to Dr. A. P. Young for many discussions concerning spin glass dynamics in $d = 2$, and for the explicit expression for the parallel correlation length exhibited in Eq. (8). This research was supported in part by the Cockrell Family Regents Chair in Engineering #12, and the Cockrell Family Dean's Chair in Engineering Excellence, both at The University of Texas at Austin. The authors also wish to thank Dr. S. K. Banerjee, NRI SWAN, and NSF NNIN for their support of this research.

-
- [1] V. S. Zotev, G. F. Rodriguez, G. G. Kenning, R. Orbach, E. Vincent, and J. Hammann, *Phys. Rev. B* **67**, 184422 (2003).
- [2] G. F. Rodriguez, Initial conditions and long time dynamics for a complex system: Hierarchical properties of the spin glass decay, Ph.D. dissertation, University of California, Riverside, 2004; G. F. Rodriguez, G. G. Kenning, and R. Orbach, *Phys. Rev. B* **88**, 054302 (2013).
- [3] Y. G. Joh, R. Orbach, G. G. Wood, J. Hammann, and E. Vincent, *J. Phys. Soc. Jpn.* **69**(Suppl. A), 215 (2000).
- [4] S. Guchhait and R. Orbach, *Phys. Rev. Lett.* **112**, 126401 (2014).
- [5] S. Franz, G. Parisi, and M. A. Virasoro, *J. Phys.* **14**, 1657 (1994).
- [6] L. W. Lee and A. P. Young, *Phys. Rev. B* **76**, 024405 (2007).
- [7] http://science.energy.gov/~media/bes/pdf/reports/files/OFMS_rpt.pdf.
- [8] G. G. Kenning, J. M. Slaughter, and J. A. Cowen, *Phys. Rev. Lett.* **59**, 2596 (1987).
- [9] G. G. Kenning, J. Bass, W. P. Pratt, Jr., D. Leslie-Pelecky, L. Hoines, W. Leach, M. L. Wilson, R. Stubi, and J. A. Cowen, *Phys. Rev. B* **42**, 2393 (1990).
- [10] L. Sandlund, P. Granberg, L. Lundgren, P. Nordblad, P. Svedlindh, J. A. Cowen, and G. G. Kenning, *Phys. Rev. B* **40**, 869(R) (1989).
- [11] P. Granberg, P. Nordblad, P. Svedlindh, L. Lundgren, R. Stubi, G. G. Kenning, D. L. Leslie-Pelecky, J. Bass, and J. Cowan, *J. Appl. Phys.* **67**, 5252 (1990).
- [12] E. Marinari, G. Parisi, J. Ruiz-Lorenzo, and F. Ritort, *Phys. Rev. Lett.* **76**, 843 (1996).
- [13] J. Kisker, L. Santen, M. Schreckenberg, and H. Rieger, *Phys. Rev. B* **53**, 6418 (1996).
- [14] P. Sibani, J. C. Schön, P. Salamon, and J.-O. Andersson, *Europhys. Lett.* **22**, 479 (1993); P. Sibani and J.-O. Andersson, *Phys. A (Amsterdam)* **206**, 1 (1994).
- [15] T. Shirakura and S. Inawashiro, *J. Phys.: Condens. Matter* **3**, 3785 (1991); Y. G. Joh, R. Orbach, G. G. Wood, J. Hammann, and E. Vincent, *Phys. Rev. Lett.* **82**, 438 (1999).
- [16] H. Rieger, *J. Phys. A: Math. Gen.* **26**, L615 (1993); H. Rieger, B. Steckemetz, and M. Schreckenberg, *Europhys. Lett.* **27**, 485 (1994).
- [17] H. Rieger, L. Santen, U. Blasum, M. Diehl, M. Jünger, and G. Rinaldi, *J. Phys. A: Math. Gen.* **29**, 3939 (1996).
- [18] H. Kawamura and H. Yonehara, *J. Phys. A: Math. Gen.* **36**, 10867 (2003).
- [19] A. P. Young (private communication).
- [20] Ph. Refregier, E. Vincent, J. Hammann, and M. Ocio, *J. Phys.* **I 48**, 1533 (1987); M. Lederman, R. Orbach, J. M. Hammann, M. Ocio, and E. Vincent, *Phys. Rev. B* **44**, 7403 (1991); J. Hammann, M. Lederman, M. Ocio, R. Orbach and E. Vincent, *Phys. A (Amsterdam)* **185**, 278 (1992); Anticipation of an effective nonergodicity that preserves the hierarchy of free-energy valleys, but allows transitions, was proposed by S. L. Ginzburg, *Zh. Eksp. Teor. Fiz.* **90**, 754 (1986) [*Sov. Phys.-JETP* **63**, 439 (1986)].
- [21] M. Mèzard, G. Parisi, N. Sourlas, G. Toulouse, and M. A. Virasoro, *Phys. Rev. Lett.* **52**, 1156 (1984); *J. Phys. (France)* **45**, 843 (1984).
- [22] D. Vertechi and M. A. Virasoro, *J. Phys. I* **50**, 2325 (1989).
- [23] S. Guchhait, M. Jamil, H. Ohldag, A. Mehta, E. Arenholz, G. Lian, A. LiFatou, D. A. Ferrer, J. T. Markert, L. Colombo, and S. K. Banerjee, *Phys. Rev. B* **84**, 024432 (2011).
- [24] T. Kasuya, in s-d and s-f interaction and rare earth metals, *Magnetism*, Vol. IIB, edited by G. T. Rado and H. Suhl (Academic, New York, 1966), pp. 215–294.
- [25] S.-k. Ma, *Phys. Rev. B* **22**, 4484 (1980).
- [26] A. Amir, Y. Oreg, and Y. Imry, *Annu. Rev. Condens. Matter Phys.* **2**, 235 (2011); *Proc. Natl. Acad. Sci. U. S. A.* **109**, 1850 (2012).
- [27] G. G. Kenning, G. F. Rodriguez, and R. Orbach, *Phys. Rev. Lett.* **97**, 057201 (2006).
- [28] A. L. Burin, D. Natelson, D. D. Osheroff, and Y. Kagan, in *Tunneling Systems in Amorphous and Crystalline Solids*, edited by P. Esquinazi (Springer, Berlin, 1998), pp. 223–316.
- [29] P. Nalbach, D. D. Osheroff, and S. Ludwig, *J. Low Temp. Phys.* **137**, 395 (2004).
- [30] D. Parker, F. Ladieu, J. Hammann, and E. Vincent, *Phys. Rev. B* **74**, 184432 (2006).
- [31] P. Nordblad, P. Svedlindh, L. Sandlund, and L. Lundgren, *Phys. Lett. A* **120**, 475 (1987).
- [32] G. Parisi, *Phys. Lett. A* **73**, 203 (1979); *Phys. Rev. Lett.* **43**, 1754 (1979); *J. Phys. A: Math. Gen.* **13**, L115 (1980).
- [33] D. S. Fisher and D. A. Huse, *Phys. Rev. B* **38**, 373 (1988); **38**, 386 (1988); **36**, 8937 (1987).
- [34] K. Gunnarsson, P. Svedlindh, P. Nordblad, L. Lundgren, H. Aruga, and A. Ito, *Phys. Rev. Lett.* **61**, 754 (1988).
- [35] P. Svedlindh, L. Lundgren, P. Nordblad, and H. S. Chen, *Europhys. Lett.* **3**, 243 (1987); P. Nordblad, L. Lundgren, P. Svedlindh, K. Gunnarsson, H. Aruga, and A. Ito, *J. Phys. (France), Colloq.* **49**, C8-1069 (1988); S. M. Rezende, F. C. Montenegro, M. D. Coutinho-Filho, C. C. Becerra, and A. Paduan-Filho, *ibid.* **49**, C8-1267 (1988); L. Lèvy, *Phys. Rev. B* **38**, 4963 (1988); E. Vincent, J. Hammann, and M. Alba, *Solid State Commun.* **58**, 57 (1986); N. Bontemps, J. Rajchenbach, R. V. Chamberlin, and R. Orbach, *Phys. Rev. B* **30**, 6514 (1984).
- [36] D. Chu, G. G. Kenning, and R. Orbach, *Philos. Mag. B* **71**, 479 (1995); D. Chu, Ph.D. dissertation, University of California, Los Angeles, 1994.
- [37] E. Vincent, J.-P. Bouchaud, D. S. Dean, and J. Hammann, *Phys. Rev. B* **52**, 1050 (1995); Y. G. Joh, R. Orbach, and J. Hammann, *Phys. Rev. Lett.* **77**, 4648 (1996); *Philos. Mag. B* **77**, 231 (1998).
- [38] J.-P. Bouchaud, *J. Phys. I* **2**, 1705 (1992); J.-P. Bouchaud and D. S. Dean, *ibid.* **5**, 265 (1995).